DESTABILIZING FORCE OF LABYRINTH SEAL

Hiroshi Kanki
Mitsubishi Heavy Industries, Ltd.
Takasago, Japan

Shigeki Morii
Mitsubishi Heavy Industries, Ltd.
Hiroshima, Japan

A great deal of research has recently been conducted to solve the subsynchronous rotor vibration problems in high-performance turbomachinery. Particularly, the destabilizing effect of the labyrinth seal on compressors or turbines has been investigated for many years (refs. 1 to 9). In spite of many efforts the dynamic effect of the labyrinth seal had not been fully determined from qualitative and quantitative points of view. But from our theoretical and experimental work, we have determined completely the dynamic characteristics of the labyrinth seal.

This paper presents the results of recent theoretical and experimental works.

We developed a theoretical study and a numerical calculation program to obtain the dynamic coefficients based on Iwatsubo's perturbation method (ref. 3) and Jenny's tangential momentum effect evaluation method (ref. 9). The simplified formulation was programmed for practical design use. Qualitative and quantitative evaluations of the computer program have been done in several published works. Our experimental study also evaluated damping coefficients and considered inlet swirl effects.

Experimental studies on the labyrinth seal have been performed to improve blading efficiency and to analyze rotor dynamics. For example, the basic labyrinth seal test was done in 1970 to verify Alford's theory, and static and semistatic tests were performed to improve design, to reduce leakage, and to evaluate cross-coupled stiffness. In 1984-1985, to confirm the phenomena, the theoretical analysis of dynamic coefficients, and the swirl effect of the labyrinth seal, we continued seal dynamic model tests. This paper presents primarily the results of the dynamic test.

SYMBOLS

a,b	displacement
C	peripheral velocity
f	cross section of seal chamber
g	gravity acceleration
h	strip height

L	length of labyrinth seal
l	length of strip pitch
n	ratio of specific heat
P	pressure
q	mass flow rate in axial direction
R	gas constant
R_S	radius of labyrinth seal
T	absolute temperature of gas in seal
t	time
U'	length of acting surface of shear (stator)
U"	length of acting surface of shear (rotor)
u	peripheral velocity of labyrinth seal, $R_S \cdot \Omega$
w	peripheral unit length, $R_S \cdot \psi$
δ	radial clearance of seal
θ_a, θ_b	angular displacement
λ'	friction coefficient (stator)
$\lambda"$	friction coefficient (rotor)
μ	strip flow coefficient
ρ	density of gas
τ'	friction shear stress of stator surface
$\tau"$	friction shear stress of rotor surface
Ω	rotating speed of rotor
ω	whirling speed of rotor

Subscripts:

a	outlet
e	entry
F	strip
i	seal chamber number or strip

x axial

Z strip number

* steady state

THEORETICAL STUDY OF DESTABILIZING FORCE CAUSED BY LABYRINTH SEAL

To investigate the destabilizing force caused by the labyrinth seal, an analytical model of the labyrinth seal was established for calculating eight dynamic coefficients (four stiffness coefficients and four damping coefficients) considering inlet swirl effects.

Modeling the Labyrinth Seal

In the flow model of the labyrinth seal Kostyuk introduced one peripheral velocity variable C in the core flow of each labyrinth chamber and developed a simple equation (ref. 5). The developed analytical method uses the modified Kostyuk equation on the labyrinth seal shown in figure 1.

The following fundamental equations are developed for the differential element of unit length showed in figure 2:

Mass Flow Rate Passing Through Strip

$$q_i^2 = \mu_i^2 \cdot \delta_i^2 \cdot (P_{i-1}^2 - P_i^2) \tag{1}$$

Mass Flow Rate Rectified in Chamber

$$\begin{aligned} 2\pi R_{SFi} \cdot q_i &= 2\pi R_{Si} \cdot q_{ei} \\ 2\pi R_{SFi+1} \cdot q_{i+1} &= 2\pi R_{Si} \cdot q_{ai} \end{aligned} \tag{2}$$

Continuous Flow Rate in Chamber

$$\frac{\partial(\rho_i f_i)}{\partial t} + f_i \cdot \frac{\partial(\rho_i C_i)}{\partial W_i} + (q_{ai} - q_{ei}) = 0 \tag{3}$$

Circumferential Momentum in Chamber

$$\frac{\partial(\rho_i f_i C_i)}{\partial t} + f_i \cdot \frac{\partial(\rho_i C_i^2)}{\partial w_i} + (q_{ai} C_{ai} - q_{ei} C_{ei}) + \tau_i' U_i - \tau_i'' U_i'' = -f_i \cdot \frac{\partial P_i}{\partial w_i} \tag{4}$$

Equation of State

$$\begin{aligned} P_i &= g\rho_i \cdot R_i \cdot T_i \\ P_i &= \rho_i^{-n_i} = \text{Const.} \end{aligned} \tag{5}$$

These equations were established for each strip and chamber. And the inlet and outlet conditions of the seal were given as follows:

$$P_o = P_{*o} = P_e \qquad P_Z = P_{*Z} = P_a \qquad T_o = T_e$$
$$P_Z = T_a \qquad C_o = C_{*o} = C_e \tag{6}$$

Method of Solution

To solve equations (1) to (5), we applied Iwatsubo's method (ref. 3), that is, the perturbation linealized method, as follows. The following nondimensional variables ξ, η, ζ, and ψ were introduced as

$$P_i = P_{*i}(1 + \xi_i), \quad C_i = C_{*i}(1 + \eta_i)$$
$$C_{ei} = C_{e*i}\ (1 + \eta_{ei}), \quad C_{ai} = C_{e,\,i+1} = C_{e*i+1}\ (1 + \eta_{e,\,i+1}) \tag{7}$$
$$q_i = q_{*i}\cdot(1 + \zeta_i), \quad \delta_i = \delta_{*i}(1 + \psi_i)$$

and, assuming that the rotor is whirling along an elliptical orbit, ψ_i is represented as

$$\psi_i = \frac{a_i}{\delta_{*i}} \cos\omega t\cdot\cos\varphi + \frac{b_i}{\delta_{*i}} \sin\omega t\cdot\sin\varphi \tag{8}$$

Rotor displacement $a*, b*$ and angular displacement θ_a, θ_b have the following relation:

$$a_i = a_* + \theta a\cdot\sum_{j=1}^{i-1} \ell_j \qquad b_i = b_* - \theta_b\cdot\sum_{j=1}^{i-1} \ell_j \tag{9}$$

Then these equations were divided into the steady-state equations and the dynamic-state equations shown in table I. As the number of variables was greater than the number of equations, the following two assumptions were made:

(1) Steady-State Tangential Momentum Parameter K_S

The parameter K_S, suggested by Jenny (ref. 9), is defined as follows:

$$C_{e*i} - C_{a*i} - Ks\cdot(C_{e*i} - C_{*i}) \tag{10}$$

This parameter is the one most important to the destabilizing force and depends on the labyrinth seal geometry.

(2) Dynamic-State Tangential Momentum Parameter K_D

In the dynamic state, a parameter K_D, different from Jenny's K_S parameter (ref. 9) as

$$\eta_{ei} = K_o \cdot \eta_i \tag{11}$$

These steady state and dynamic state differential equations yield to the algebraic linear equations with eight coefficients K_{xx}, K_{xy}, K_{yx}, K_{yy}, C_{xx}, C_{xy}, C_{yx}, and C_{yy} by Iwatsubo's method (ref. 3).

And assuming that the rotor is at the center of the labyrinth seal, the coefficients satisfy the next condition

$$\circ\ K_{xx} = K_{yy},\quad K_{xy} = -K_{yx},\quad C_{xx} = C_{yy},\quad C_{xy} = -C_{yx} \tag{12}$$

Numerical Analysis and Comparison Between Theory and Published Experimental Results

Two experiments on labyrinth seal destabilizing force have been published: Wright's (ref. 1), on the effect of bore taper; and Benckert's (ref. 12), which clarified the effect of entry swirl. First, the analytical results of using the preceding method are compared with Wright's experimental results. The configuration of the seal is shown in figure 3. The calculated and measured dynamic coefficient data are shown in figures 4 and 5. The calculation was performed with respect to the experimental data on the effects of taper bore. The taper bore effect is summarized in table II.

The second step compares the calculated results with Benckert's experimental results for the full labyrinth seal. As shown in figure 6, the calculated results and Benckert's experimental results are compared using Benckert's nondimensional variables K^*_0, E^*_0 as follows.

$$K_o^* = \frac{K_{xy}}{\dfrac{(P_Z - P_o)\cdot R_s \cdot L}{\delta}} \tag{13}$$

$$E_o^* = \frac{\rho_o}{2} C_o^2 \Big/ \left(P_Z - P_o + \frac{\rho_o}{2} C_{axo}^2\right) \tag{14}$$

The calculation and experiment have a good agreement. The calculated entry swirl effect is also shown in table II.

EXPERIMENTAL STUDY OF SMALL LABYRINTH SEAL MODEL

A small labyrinth seal model was tested to qualitatively confirm labyrinth seal dynamics. The experimental model is shown in figure 7. The model casing had four nozzles attached to the annular chamber of the labyrinth seal in the tangential direction (ref. 7). The inlet swirl could be alternated by nozzle selection for each test condition. The dimensions of the model labyrinth seal are summarized in table III. The model was designed to demonstrate the occurrence of whirl at relatively low pressure.

The main test items are summarized in table IV. The tests measured system damping for each test condition. The effect of shaft rotation is very small because of the size of the model and the limit of the rotating speed. Therefore most tests were preformed in nonrotating conditions. System damping was measured by perturbing test working conditions. The free vibration decay was measured for each test. The following results were obtained from this series of tests.

Effect of Labyrinth Seal on Rotor Stability

Figure 8 shows the typical test results for the original straight seal. System damping varied according to nozzle inlet pressure. The nozzle inlet pressure represents the seal inlet swirl velocity. The seal inlet pressure was about one-half of the nozzle inlet pressure.

The measured damping ratio tended to increase up to 0.2 kgf/cm^2, to decrease as pressure increased, and to fall into the unstable region for pressure over 0.5 kgf/cm^2. The vibration waves in figure 8 clearly show the change of system damping.

Effect of the Labyrinth Seal on Damping

Figure 9 shows test results at the no-swirl condition for the original straight seal. The damping increased with inlet pressure and the natural frequency slightly decreased. This shows that the seal has a direct effect on damping.

Effect of Tapered bore

Figure 10 shows the test results for the simplified tapered-bore seal. The clearances were changed for half the number of seal fins so that the seal would simulate both a convergent and a divergent seal. For this model the convergent seal showed more stable characteristics than the divergent seal. However, the differences between them were very small.

Effect of Swirl Breaker

To reduce the destabilizing effect of inlet swirl, two types of swirl breaker were tested. The one had radial bypass holes and the other had antiswirl bypass holes. The results (fig. 11) show a significant increase in stability limit for both cases, and with the antiswirl breaker the stable condition could be maintained to about four times the inlet pressure.

Comparison of Test Results with Calculated Results

Figure 12 shows the nondimensional destabilizing effect (by Benckert's method) for swirl test results and analytical values for conditions associated with the original straight seal model and with tapered-bore seal models. The figure shows fairly good agreement between the theory and the experiment for both the qualitative and quantitative points of views.

EXAMPLE OF APPLICATION

The method of calculating labyrinth seal dynamics was applied to solve compressor vibration problems (ref. 10).

When the compressor was replaced by a new machine with improved performance the machine experienced severe unstable subsynchronous whirl over 90 percent load. The stability characteristics were analyzed by the Mitsubishi rotor dynamics program (ref. 11). The middle of figure 13 shows the stability graph of this rotor system; the graph includes the labyrinth seal destabilizing effects calculated by this work.

After lengthy discussions of the analytical results and the observed phenomena, we decided on a countermeasure, the installation of a damper bearing. A one-day shutdown of the compressor allowed the damper bearing to be installed without unbolting the compressor casing. When the compressor was run with the damper bearing, the subsynchronous vibration completely disappeared. The top and bottom figure of figure 13 compare vibration records from before and after damper bearing installation.

CONCLUSIONS

Our theoretical and experimental study of the destabilizing force of the labyrinth seal confirmed the following dynamic characteristics:

1. The unstable vibration phenomena of labyrinth seals are clearly demonstrated by a simple model rotor system.

2. The existence of the damping effect in labyrinth seals is confirmed in the absence of inlet swirl.

3. For this model the tapered clearance of the labyrinth seal has little effect on the destabilizing force.

4. The special swirl breaker showed a reasonable reduction of the destabilizing effect of the labyrinth seal.

5. Application of the results of the stability analysis gave a reasonable interpretation for actual turbomachinery vibration phenomena.

REFERENCES

1. Benckert, H.; and Wachter, J.: Flow Induced Spring Constants of Labyrinth Seals. I. Mech. E, Sept. 1980. (See also NASA CP-2338, pp. 189-212.)

2. Childs, D.; and Dressman, J.: Testing of Turbulent Seals for Rotordynamic Coefficients. Rotordynamic Instability Problems in High-Performance Turbomachinery, NASA CP-2250, 1982, pp. 157-171.

3. Iwatsubo, T.; et al.: Flow Induced Force of Labyrinth Seal. Rotordynamic Instability Problems in High-Performance Turbomachinery, NASA CP-2250, 1982, pp. 205-222.

4. Kurohashi, M.; et al.: Spring and Damping Coefficients of Labyrinth Seals. Proceedings I. Mech. E., 1980.

5. Kostyuk, A.: Theoretical Analysis of Aerodynamic Forces in Labyrinth Glands of Turbomachines. Teploenergetika, 1972.

6. Wright, D.V.: Air Model Test of Labyrinth Seal Forces on a Whirling Rotor. ASME, Eng. Power, Oct. 1978.

7. Leong, Y.M.M. Salman; Brown, R.D.: Experimental Investigations of Lateral Forces Induced by Flow through Model Labyrinth Glands. Rotordynamic Instability Problems in High-Performance Turbomachinery, NASA CP-2338, 1984, pp. 187-210.

8. Miller, E.H.; and Vohr, J.H.: Preliminary Investigation of Labyrinth Packing Pressure Drops at Onset of Swirl-Induced Rotor Instability. Rotordynamic Instability Problems in High-Performance Turbomachinery, NASA CP-2338, 1984, pp. 281-294.

9. Jenny, R.: Labyrinths as a Cause of Self-excited Rotor Oscillations in Centrifugal Compressors. Sulzer Technical Review 4, 1980.

10. Morii, S.; Nishimoto, K.; and Kanki, H.; et al.: On the Subsynchronous Whirl in the Centrifugal Compressor. ICVPE, 1986. To be published.

11. Shiraki, K.; and Kanki, H.: A New Vibration Criteria for High Speed Large Capacity Turbomachinery. Proceeding of the Eighth Turbomachinery Symposium.

12. Wright, D.V.: Labyrinth Seal Forces on a Whirling Rotor. ASME, AMD-Vol. 55, 1983.

TABLE I. - LINEALIZED EQUATION OF LABYRINTH SEAL

Circumferential Momentum Equation

$$\frac{f_{*i}}{n}\frac{\partial \xi_i}{\partial t} + f_{*i}\frac{\partial \eta_i}{\partial t} + \frac{f_{*i}}{R_{si}}\left(\frac{gR_iT_i}{C_{*i}} + \frac{C_{*i}}{n}\right)\frac{\partial \xi_i}{\partial \varphi} + \frac{2f_{*i}C_{*i}}{R_{si}}\frac{\partial \eta_i}{\partial \varphi}$$

$$- \frac{gR_iT_iP^2_{*i+1}\mu^2_{i+1}\delta^2_{*i+1}Ce_{*i+1}R^2_{sFi+1}}{q_{e*i}P_{*i}C_{*i}R^2_{si}}\xi_{i+1}$$

$$+ \left[\frac{gR_iT_iP_{*i}}{q_{e*i}C_{*i}R^2_{si}}(\mu^2_{i+1}\delta^2_{*i+1}Ce_{*i+1}R^2_{SFi+1} + \mu^2_i\delta^2_{*i}Ce_{*i}R^2_{SFi})\right.$$

$$\left. + \frac{1}{2}\{\lambda'_iU'_i|C_{*i}| - \lambda''_iU''_i|u_i - C_{*i}|(\frac{u_i}{C_{*i}} - 1)\}\right]\xi_i$$

$$- \frac{gR_iT_iP_{*i-1}\mu^2_i\delta^2_{*i}Ce_{*i}R^2_{SFi}}{q_{e*i}P_{*i}C_{*i}R^2_{si}}\xi_{i-1} + \frac{gR_iT_iq_{e*i}Ce_{*i+1}}{P_{*i}C_{*i}}\eta_{ei+1}$$

$$+ \{\lambda'_iU'_i|C_{*i}| + \lambda''_iU''_i|u_i - C_{*i}|\}\eta_i - \frac{gR_iT_iq_{e*i}Ce_{*i}}{P_{*i}C_{*i}}\eta_{ei}$$

$$= \frac{gR_iT_i}{2q_{e*i}P_{*i}C_{*i}R^2_{si}}\{\mu^2_{i+1}\delta_{*i+1}Ce_{*i+1}R^2_{SFi+1}(P^2_{*i} - P^2_{*i+1}) - \mu^2_i\delta_{*i}Ce_{*i}R^2_{SFi}(P^2_{*i-1} - P^2_{*i})\}$$

$$\{a_*\cos(\varphi+\omega t) + a_*\cos(\varphi-\omega t) - b_*\cos(\varphi+\omega t) + b_*\cos(\varphi-\omega t)\}$$

$$+ \frac{\omega\ell_i}{2}\{-a_*\sin(\varphi+\omega t) + a_*\sin(\varphi-\omega t) + b_*\sin(\varphi+\omega t) + b_*\sin(\varphi-\omega t)\}$$

$$+ \frac{gR_iT_i}{2q_{e*i}P_{*i}C_{*i}R^2_{si}}\{\mu^2_{i+1}\delta^2_{*i+1}Ce_{*i+1}R^2_{SFi+1}(P^2_{*i} - P^2_{*i+1})\sum_{j=1}^{i}\ell_j$$

$$- \mu^2_i\delta_{*i}Ce_{*i}R^2_{SFi}(P^2_{*i-1} - P^2_{*i})\sum_{j=1}^{i-1}\ell_j\}$$

$$\{\theta_a\cos(\varphi+\omega t) + \theta_a\cos(\varphi-\omega t) - \theta_b\cos(\varphi+\omega t) + \theta_b\cos(\varphi-\omega t)$$

$$+ \frac{\omega\ell_i}{2}\left(\sum_{j=1}^{i}\ell_j - Si\ell_i\right)\{-\theta_a\sin(\varphi+\omega t) + \theta_a\sin(\varphi-\omega t) + \theta_b\sin(\varphi+\omega t) + \theta_b\sin(\varphi-\omega t)\}$$

TABLE I. - CONCLUDED.

Steady State Equation

- Mass Flow Rate Equation

$$\frac{q_i^2}{\mu_i^2 \delta_i^2} = P_{i-1}^2 - P_i^2$$

- Continuous Equation

$$R_{SFi} q_i = R_{Si} q_{ei} = R_{SFi+1} q_{i+1}$$

- Circumferential Momentum Equation

$$q_{e*i}(C_{e*i+1} - C_{e*i}) + \frac{1}{2} \frac{\lambda_i' u_i'}{g R_i T_i} P_{*i} |C_{*i}| C_{*i}$$

$$- \frac{1}{2} \frac{\lambda_i' u_i'}{g R_i T_i} P_{*i} |u_i - C_{*i}| (u_i - C_{*i}) = 0$$

Dynamic State Equation

- Continuous Equation

$$\frac{f_{*i}}{n} \frac{\partial \xi_i}{\partial t} + \frac{C_{*i} f_{*i}}{R_{Si} \cdot n} \frac{\partial \xi_i}{\partial \varphi} + \frac{C_{*i} f_{*i}}{R_{Si} \cdot n} \frac{\partial \eta_i}{\partial \varphi} - \frac{g R_i T_i P_{*i+1}^2 \mu_{i+1}^2 \delta_{*i+1}^2 R_{SFi+1}^2}{q_{e*i} P_{*i} R_{si}^2} \xi_{i+1}$$

$$+ \frac{g R_i T_i P_{*i}}{q_{e*i} R_{si}^2} (\mu_{i+1}^2 \delta_{*i+1}^2 R_{SFi+1}^2 + \mu_i^2 \delta_{*i}^2 R_{SFi}^2) \xi_i - \frac{g R_i T_i P_{*i-1}^2 \mu_i^2 \delta_{*i}^2 R_{SFi}^2}{q_{e*i} P_{*i} R_{si}^2} \xi_{i-1}$$

$$= \frac{u\, g R_i T_i}{2 q_{e*i} R_{*i} R_{si}^2} \{\mu_{i+1}^2 \delta_{*i+1} R_{SFi+1}^2 (P_{*i}^2 - P_{*i+1}^2) - \mu_i^2 \delta_{*i} R_{SFi}^2 (P_{*i-1}^2 - P_{*i}^2)\}$$

$$\{a_* \cos(\varphi + \omega t) + a_* \cos(\varphi - \omega t) - b_* \cos(\varphi + \omega t) + b_* \cos(\varphi - \omega t)\}$$

$$+ \frac{\omega \ell_i}{2} \{-a_* \sin(\varphi + \omega t) + a_* \sin(\varphi - \omega t) + b_* \sin(\varphi + \omega t) + b_* \sin(\varphi - \omega t)\}$$

$$+ \frac{g R_i T_i}{2 q_{e*i} P_{*i} R_{si}^2} \{\mu_{i+1}^2 \delta_{*i+1} R_{SFi+1}^2 (P_{*i}^2 - P_{*i+1}^2) \sum_{j=1}^{i} \ell_j - \mu_i^2 \delta_{*i} R_{SFi}^2 (P_{*i-1}^2 - P_{*i}^2) \sum_{j=1}^{i-1} \ell_j\}$$

$$\{\theta a \cos(\varphi + \omega t) + \theta a \cos(\varphi - \omega t) - \theta b \cos(\varphi + \omega t) + \theta b \cos(\varphi - \omega t)\}$$

$$+ \frac{\omega \ell_i}{2} \left(\sum_{j=1}^{i} \ell_j - S_i \ell_i\right) \{-\theta a \sin(\varphi + \omega t) + \theta a \sin(\varphi - \omega t) + \theta b \sin(\varphi + \omega t) + \theta b \sin(\varphi - \omega t)\}$$

TABLE II. - SUMMARY OF CASE STUDY

	Tapered bore seal (Diverging - straight - converging)	Entry swirl (backward - forward)
K_{xx}	——→ Rigid	- - - - → A little rigid
K_{xy}	——→ Destabilizing for forward swirl	(-) (+) Destabilizing ——→ for forward swirl
C_{xx}	——→ Stabilizing	Positive and almost independent of entry swirl
C_{xy}	Rigid for forward swirl ←——	Positive and almost independent of entry swirl

TABLE III. - SPECIFICATION OF TEST MODEL

Seal diameter, mm	100
Seal radial clearance, mm	0.25
Height of seal fin, mm	2.75
Pitch of seal fin, mm	4.00
Numbers of fins	15x2
Inlet pressure, atm, absolute	1 to 3.2
Discharge pressure, atm, absolute	1
Critical speed, rpm	930

TABLE IV. - TEST ITEMS AND OBJECTIVES

Test items		Objective
Original	Swirl effect	Effect of inlet swirl
	Rotation effect	Effect of rotation of rotor
	Clearance effect	Effect of seal clearance of same configuration
	Tapered clearance effect	Effect of convergent and divergent clearance configuration
With swirl breaker	Swirl breaker effect	Effect of specially designed swirl breaker

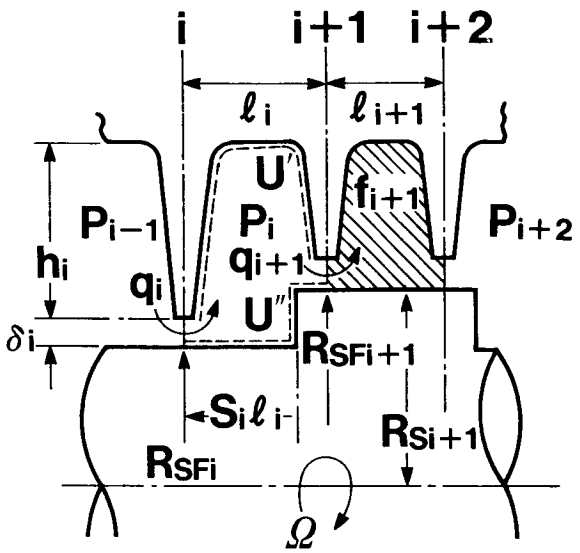

Figure 1. - Labyrinth seal.

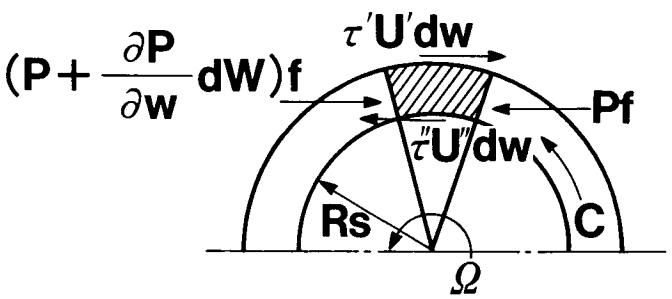

Figure 2. - Cross section of chamber.

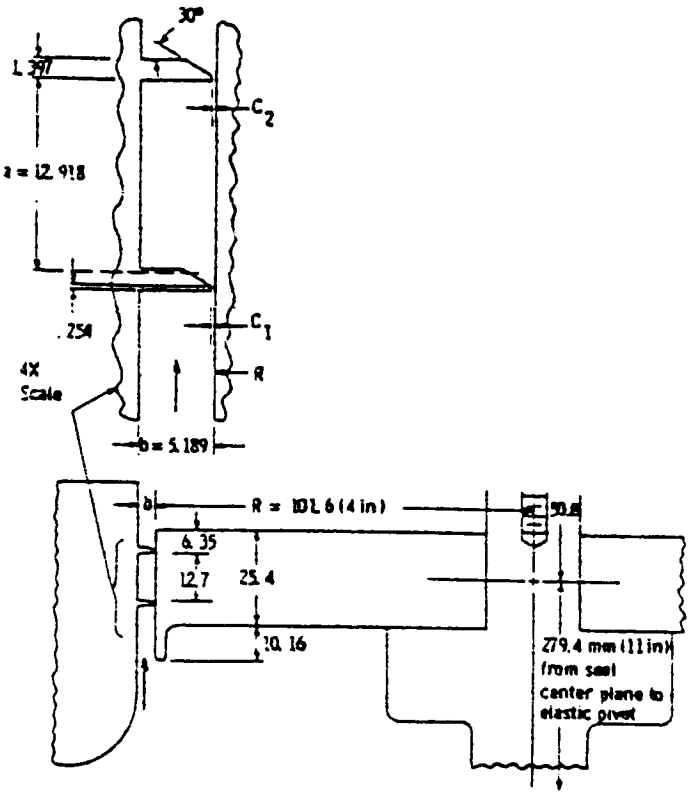

Revolution Speed : 1800rpm

Seal Type	C_2/C_1	C_1 (mm)	C_2 (mm)
Diverging	1.4973	0.1311	0.1963
Straight	1.0	0.1585	0.1585
Converging	0.6642	0.1915	0.1272

Outlet Pressure : 1.076kgf/cm²

Figure 3. - Seal configurations by Wright's test (ref. 12).

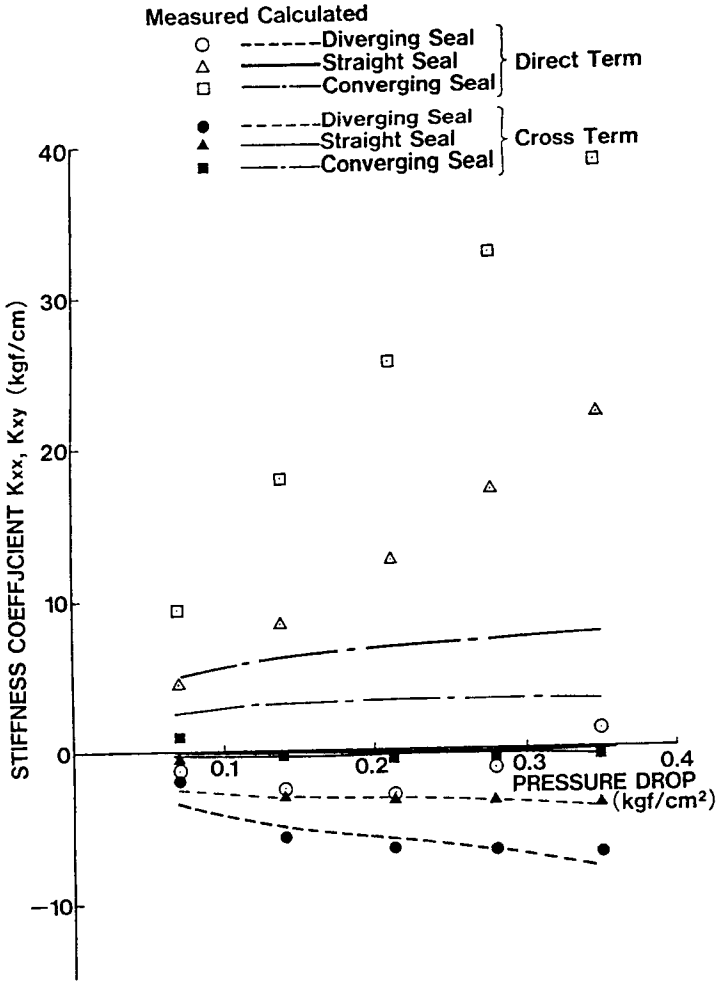

Figure 4. - Comparison of calculated and measured stiffness coefficients.

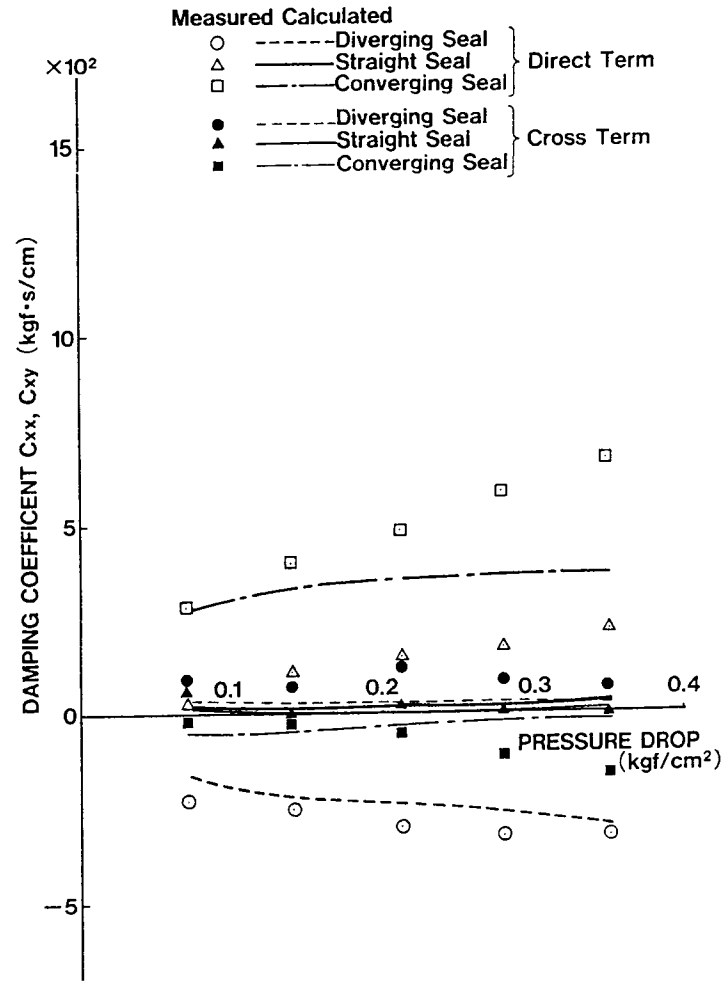

Figure 5. - Comparison of calculated and measured damping coefficients.

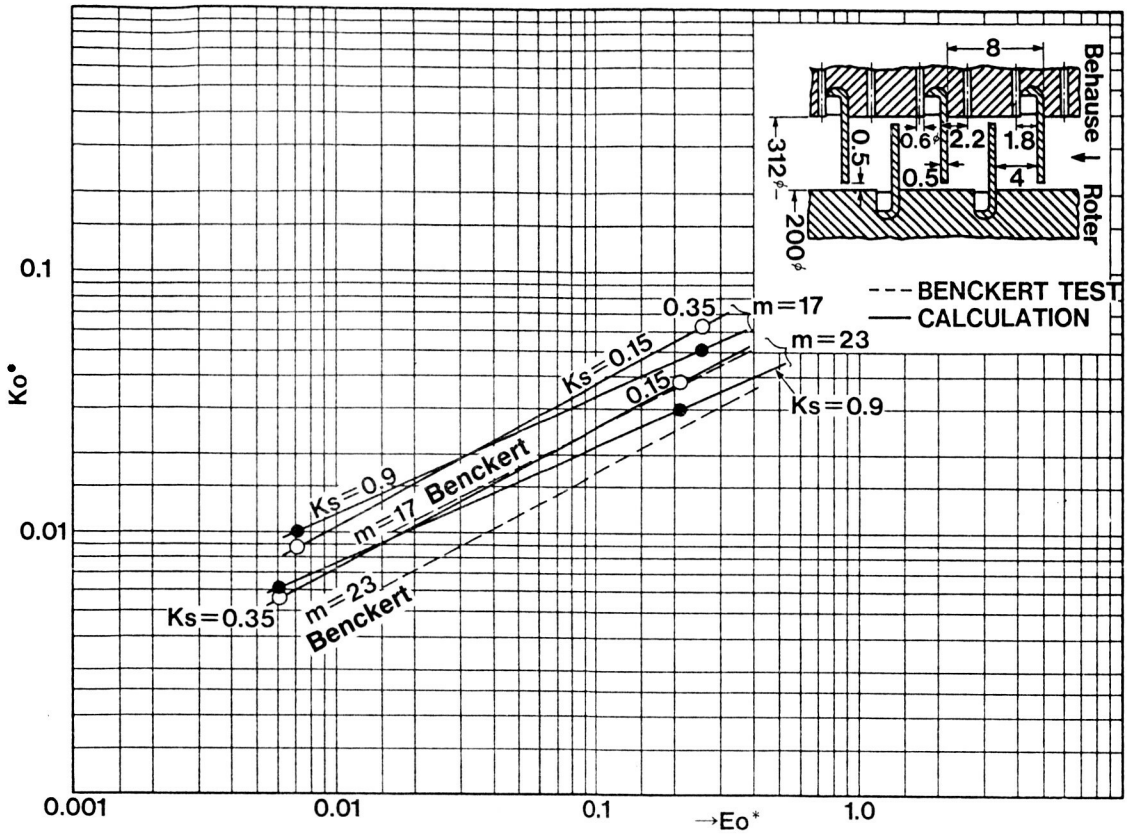

Figure 6. - Comparison of calculated cross-coupling coefficient with that measured by Benckert's test (ref. 1).

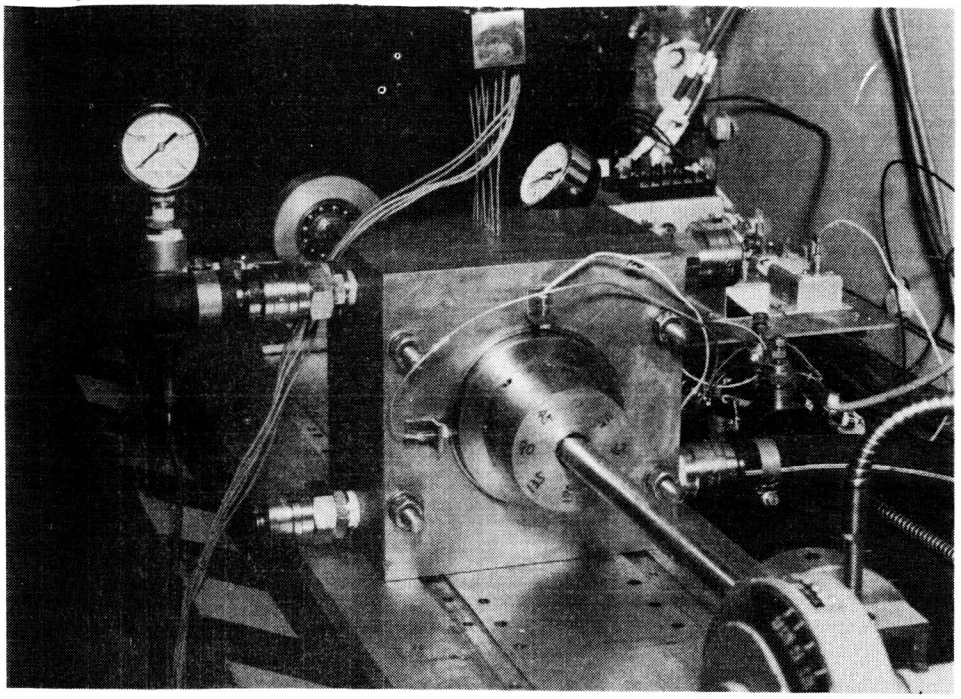

Figure 7. - Test model.

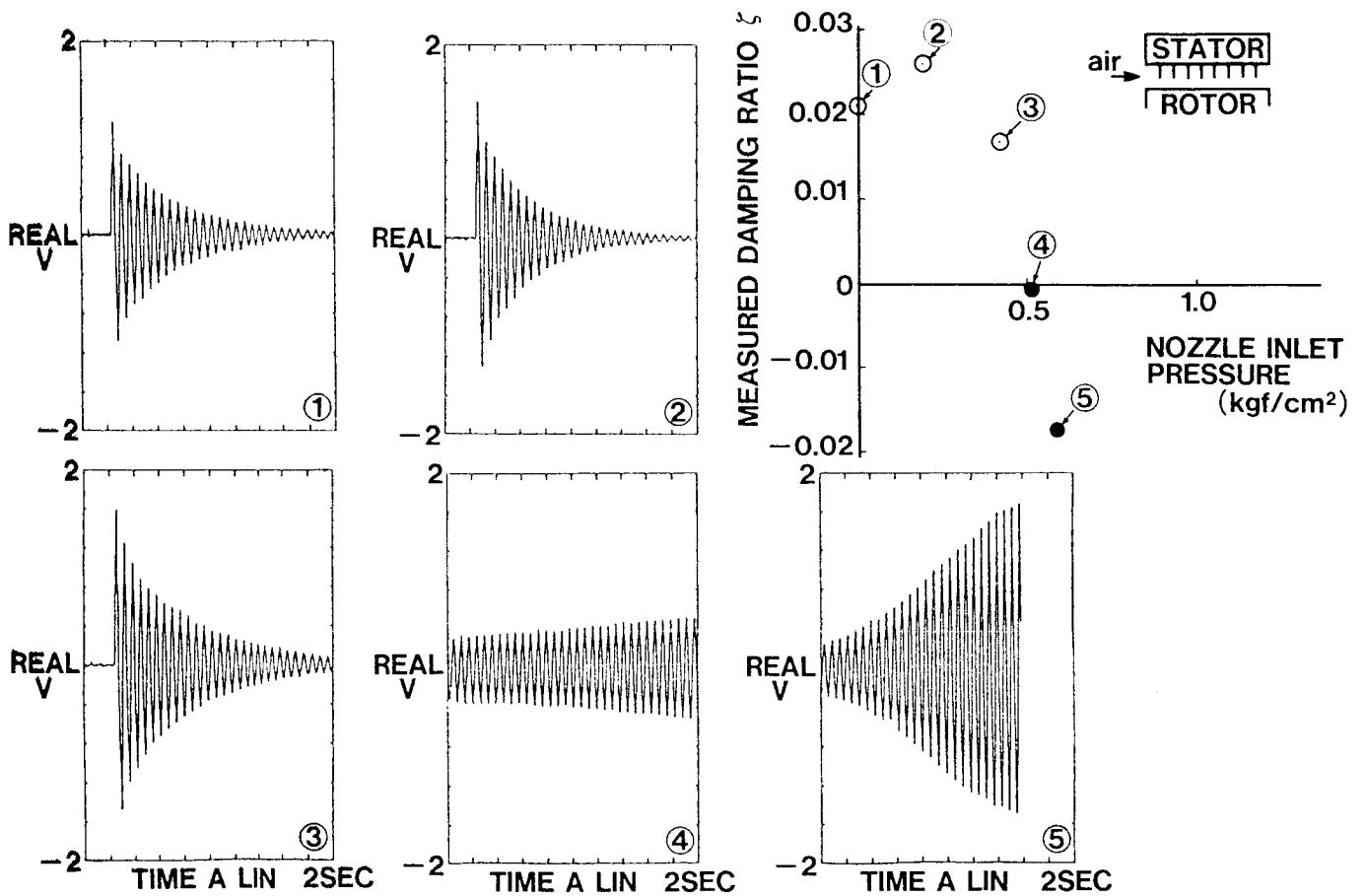

Figure 8. - Typical dynamic test results for straight seal.

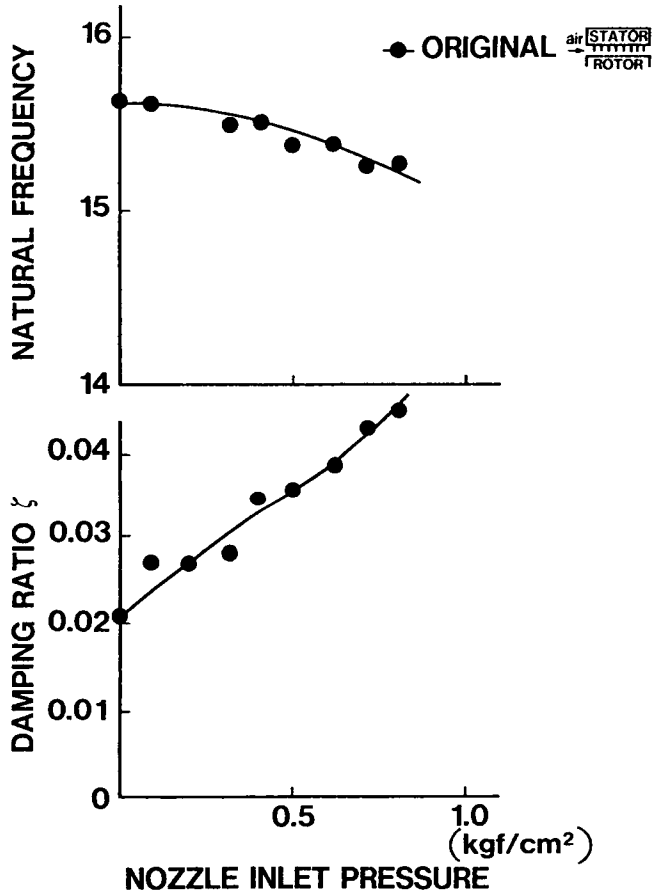

Figure 9. - Test results for nonswirl condition.

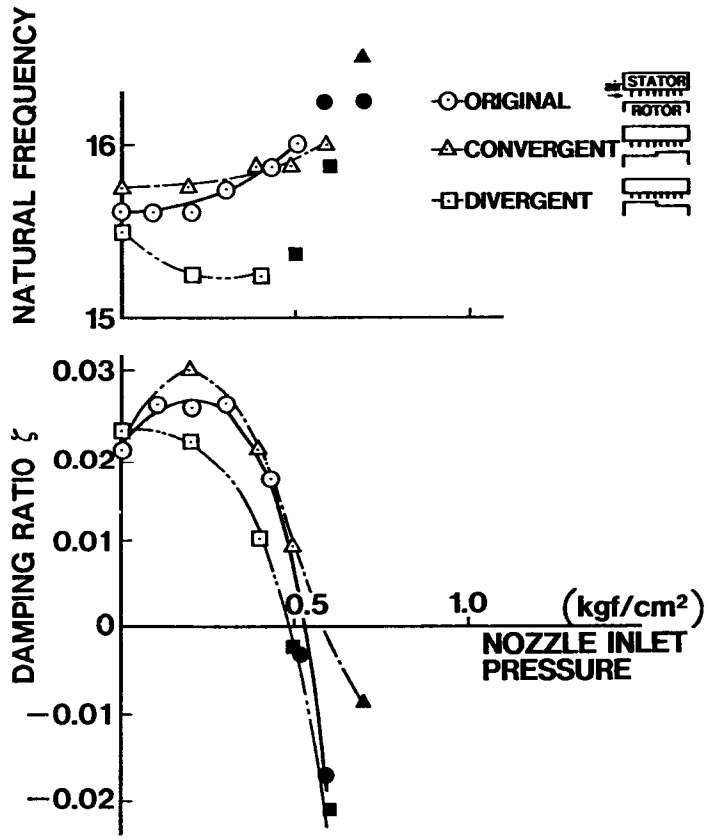

Figure 10. - Test results for swirl condition.

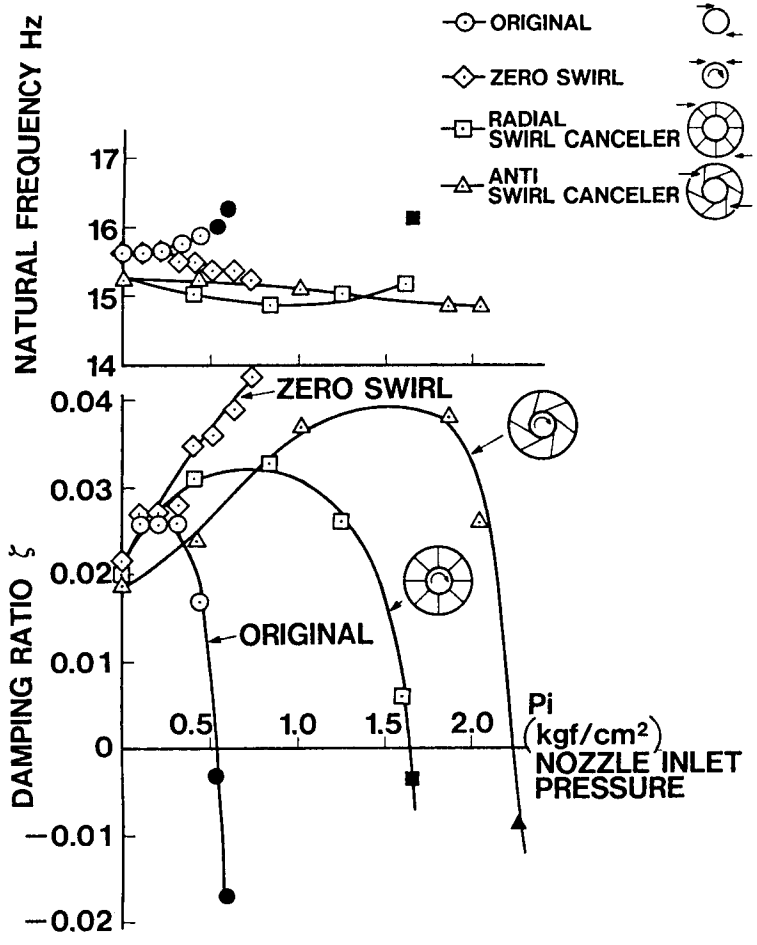

Figure 11. - Effect of swirl breaker.

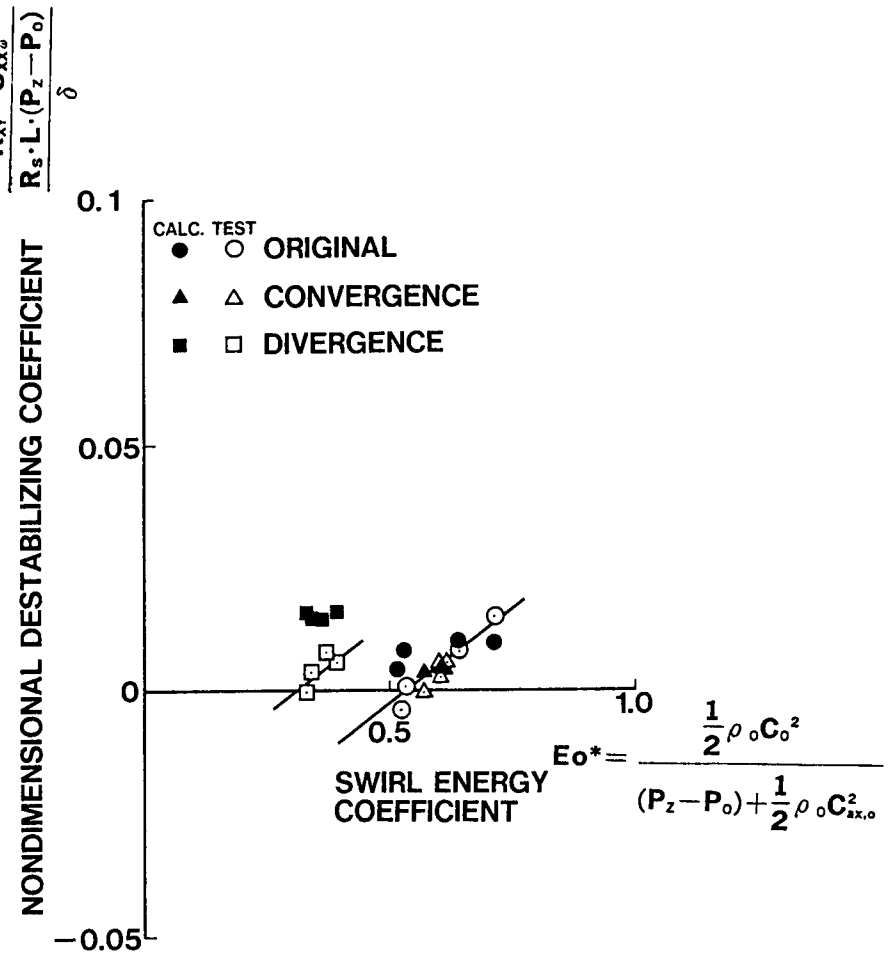

Figure 12. - Nondimensional comparison of test results and calculation.

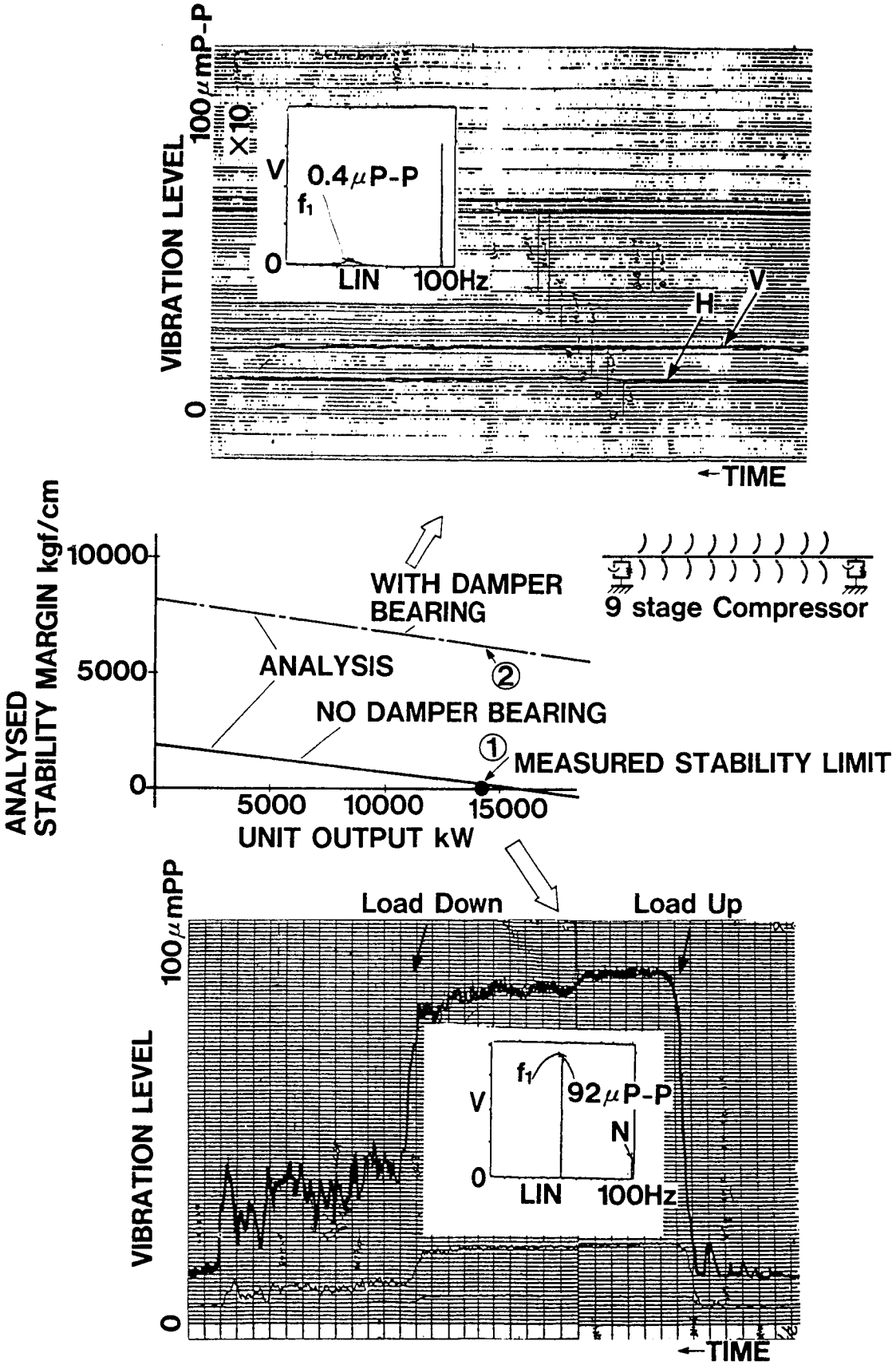

Figure 13. - Example of application of damper bearing to centrifugal compressor.